ACS OMEGA

http://pubs.acs.org/journal/acsodf

Article

Efficient Dye Degradation and Antibacterial Activity of Carbon Dots/Chitosan-Doped La_2O_3 Nanorods: In Silico Molecular Docking Analysis

Sumaira Rasool, Muhammad Imran,* Ali Haider,* Anum Shahzadi, Walid Nabgan, Iram Shahzadi, Francisco Medina, Mohammed M. Algaradah, Ahmed M. Fouda, Ali Al-Shanini,* and Muhammad Ikram*

Cite This: *ACS Omega* 2023, 8, 25401−25409

Read Online

ACCESS | Metrics & More | Article Recommendations | Supporting Information

ABSTRACT: This work demonstrates the degradation of toxic RhB (rhodamine B) dye from polluted water in various pH environments. It assesses the antibacterial action of CDs (carbon dots)/CS (chitosan)-doped La_2O_3 (lanthanum oxide) NRs (nanorods). CS and CDs have been introduced as dopants to modify the characteristics of La_2O_3 to achieve efficient outcomes. The influence of doping on the structural, morphological, optical, and elemental properties of synthesized La_2O_3 NRs was investigated through a number of analytical techniques. The structural analysis of XRD revealed a hexagonal phase. The rod-like structure of pure La_2O_3 and reduction in the size of NRs upon doping were exhibited by TEM micrographs. From UV−vis spectroscopy, increased absorption upon doping and introduction of redshift that led to reduced bandgap energy were observed. The FTIR spectra indicate the presence of functional groups of pure and integrated samples. The catalytic activity of specimens in basic medium toward dye showed excellent results (94.57%). The inhibition zone of diameter 4.15 mm was evaluated by 6 mL of CDs/CS-doped La_2O_3 NRs against *Escherichia coli* once the surface area increased by dopants. In silico experiments were performed for enoyl-[acyl-carrier-protein] reductase (FabI) and DNA gyrase enzymes to assess the potency of CS-doped La_2O_3 and CDs/CS-doped La_2O_3 as their inhibitors and to justify their possible mechanism of action.

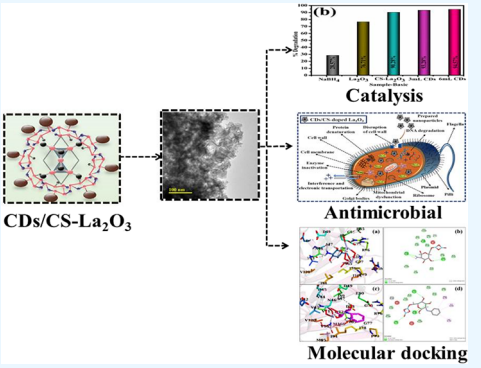

1. INTRODUCTION

All biological entities require freshwater, but worldwide water resource contamination has increased due to rapid industrialization and colossal population growth.[1] Heavy metals and toxic dyes are significant sources of water contamination that seriously threaten the natural ecosystem and human society.[2] Furthermore, poisonous microbes present in water as bacteria, fungi, algae, plankton, and amoebas cause several waterborne diseases.[3] Drinking polluted water causes numerous diseases, namely, diarrhea, tooth and bone cancer, hepatitis, typhoid, dysentery, and aquatic illness, and even death.[4] Multiple chemical, biological, and physical solutions have been developed to tackle this environmental concern. Chemical reduction is the simplest, quick, and most effective method for reducing dyes from aqueous solutions.[5] Catalysis is an essential technique based on nanomaterial semiconductors because of its low toxicity, chemical stability, and environmental friendliness.[6]

The latest research has focused on rare earth metal oxides, i.e., Y_2O_3, Gd_2O_3, Sm_2O_3, Ce_2O_3, and La_2O_3, owing to their diverse features and applications in the emerging field of dye degradation.[7] Lanthanum (La) has some advantages over the whole rare-earth-metal family in terms of high affinity to oxygen and relatively small radius.[8] However, it has no biological function in the living body, and soft metal (La) is necessary for microbicidal activity. Pearson classified La^{3+} as Lewis acid, which seems especially nontoxic and environmentally beneficial. Considering their specific affinity, La^{3+}-based compounds were employed to eliminate hazardous ions from water through adsorption.[9] In previous work, several doping agents, namely, Ag, Eu, Fe, Ni, and Cu, modify the features of La_2O_3 to accomplish the desired outcomes.[10] Complete decolorization of RhB dye occurs after 270 min in neutral and 330 min in acidic medium with binary metal oxide CeO_2/La_2O_3.[11] Arshad et al. reported that Ni-doped La_2O_3 reveals the highest photocatalytic degradation of 99.15% in 30

Received: April 26, 2023
Accepted: June 12, 2023
Published: July 3, 2023

min.[12] According to He et al., GO-doped La_2O_3 exhibited a degradation potential for RhB of 63.2% in 15 min.[13]

Nanocomposites consisting of metal oxides and conducting polymers are promising catalysts that increase the degradation rate via the synergistic effects between the metal oxide and the conducting polymer and metal oxide.[14,15] Chitosan (CS) has amino and hydroxyl functional groups consisting of *N*-acetyl glucosamine and glucosamine, which are highly significant for composite formation with metal oxides.[16] CS is a natural polymer applied as a substrate for nano-semiconductor oxide due to its chemical stability and biodegradability. The presence of a carbon substrate increased e^- mobility in conjugated carbon atoms. The number of defects in carbonaceous materials improved the photocatalytic reaction.[17] Carbon dots (CDs), one of the most favorable classes of carbon nanomaterials, have piqued the interest of researchers owing to their large specific surface area, the abundance of surficial functionalities, as well as their rich π-domains, which allow CDs to efficiently interact with organic molecules and metal ions, potentially leading to applications in wastewater purification.[18] Using a coprecipitation technique, this study prepared dope-dependent (3 and 6 mL of CDs and CS) La_2O_3 nanorods (NRs) to test the RhB dye degradation and antimicrobial activity supported by an in silico molecular docking study. The characteristic alteration in the La_2O_3 lattice with doping agents CS and CDs polymers has been predicted as an outstanding technique for gaining better CA at short time intervals, contrary to RhB dye, which has not recently been published to the best of our understanding. In addition, the effect of CS and CDs on the chemical components and structural, optical, and morphological aspects of La_2O_3 was investigated.

2. EXPERIMENTAL SECTION

2.1. Materials. Lanthanum nitrate hexahydrate ($La(NO_3)_3 \cdot 6H_2O$, 99.9%), CS ($C_6H_{11}NO_4$, 75%−85%), and sodium hydroxide (NaOH, 98%) were acquired from Sigma-Aldrich (Germany). Deionized (DI) water and CDs were used. Every chemical was consumed in its genuine state.

2.2. Synthesis of CDs. A hydrothermal carbonization approach was adopted to synthesize CDs, as elaborated in Figure 1a. Extracted lemon juice (40 mL) was taken into a Teflon-lined stainless steel and autoclaved at 120 °C for 12 h. The autoclave was spontaneously cooled to ambient temperature after the reaction, and the dark-brown-colored solution was obtained, which indicates the formation of CDs. Moreover, the solution was filtered to free the sample from impurities.[19]

2.3. Synthesis of Dopant-Free and CDs/CS-Doped Lanthanum Oxide (La_2O_3). The coprecipitation strategy was manifested for La_2O_3 NRs. $La(NO_3)_3 \cdot 6H_2O$ (1 M) was heated at 80 °C with robust stirring for 30 min. Afterward, a fixed quantity of CS (3 mL) was incorporated into the La_2O_3 solution. Then, different doping concentrations (3 and 6 mL) of CDs were integrated into the solution above with appropriate heating and continuous stirring. The precipitation agent (NaOH) (1 M) was integrated drop by drop to maintain pH ∼12, and at 7000 rpm, the sediments were isolated by centrifugation with DI water after 60 min. Subsequently, the acquired solution was heated overnight at 150 °C and then pulverized into fine powder of La_2O_3, CS-doped La_2O_3, and (3 and 6 mL) CDs/CS-doped La_2O_3 (Figure 1b).

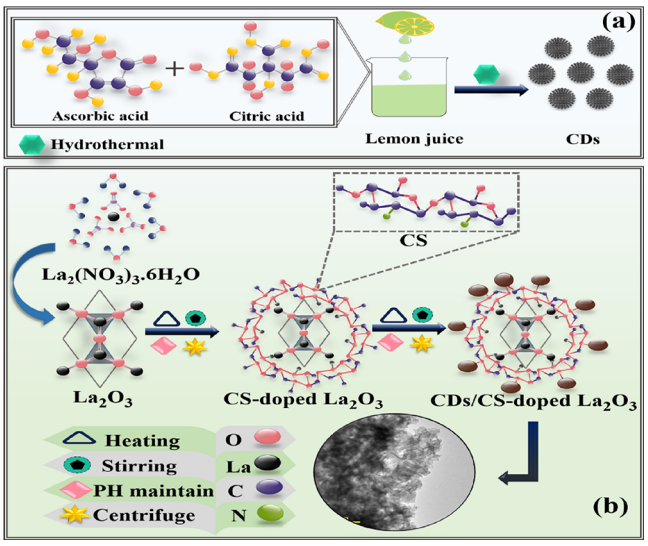

Figure 1. (a, b) Schematic illustration for preparing (a) CDs and (b) CDs/CS-doped La_2O_3 NRs.

2.4. Catalytic Activity (CA). Degradation of an oxidizing dye (RhB) with a reducing agent ($NaBH_4$) for doped and doped free La_2O_3 nanocatalysts (NCs) was measured through CA. All the reagents (RhB colorant and $NaBH_4$) were used immediately after preparation to sustain experimental purity. $NaBH_4$ solution (400 μL) was mixed in 3 mL of aqueous solution of RhB dye, and the absorption spectra were detected at regular intervals. Afterward, 400 mL of produced NCs solution was poured into RhB aqueous solution. At specified intervals, degradation was observed between 200 and 800 nm wavelength via a UV−vis spectrophotometer.

2.5. Isolation and Identification of MDR *Escherichia coli*. *2.5.1. Sample Collection.* Direct milking into sterile glassware was used to collect raw milk samples from lactating cows marketed at the marketplace, veterinary facilities, and farms in Punjab. After collection at 4 °C, raw milk was promptly carried to the lab, and MacConkey agar was used to count the *E. coli* in raw milk. All plates were kept for 48 h at 37 °C.

2.5.2. Identification and Characterization of Bacterial Isolates. Based on colonial morphology, *E. coli* has been identified through Gram staining and many biochemical assays following Bergey's Deterministic Bacteriology Manual.[20]

2.5.3. Antibiotic Susceptibility. Bauer et al. used the disc diffusion approach to conduct an antibiotic susceptibility test on Mueller Hinton agar (MHA). The experiment was implemented to investigate *E. coli* antibiotic resistance: imipenem (Imi) 10 μg (carbapenems), ceftriaxone (Cro) 30 μg (cephalosporins), amoxicillin (A) 30 μg (penicillins), ciprofloxacin (Cip) 5 μg (quinolones), tetracycline (Te) 30 μg (tetracyclines), gentamicin (Gm) 10 μg (aminoglycosides), and azithromycin (Azm) 15 μg (macrolides).[21] Purified *E. coli* culture was grown and adapted to 0.5 McFarland opacity. On MHA, antibiotic discs were positioned far from the incubation plate's surface to protect inhibitory zones from overlapping (Oxoid Limited, Basingstoke, UK). Inoculation of plates for 24 h at 37 °C and the outcomes were evaluated corresponding to the Clinical and Laboratory Standards Institute.[22] MDR bacteria were shown to resist at least three drugs.[23]

2.5.4. Antibacterial Activity. Ten MDR *E. coli* isolates from mastitic milk were evaluated for in vitro antibacterial activity

https://doi.org/10.1021/acsomega.3c02812
ACS Omega 2023, 8, 25401−25409

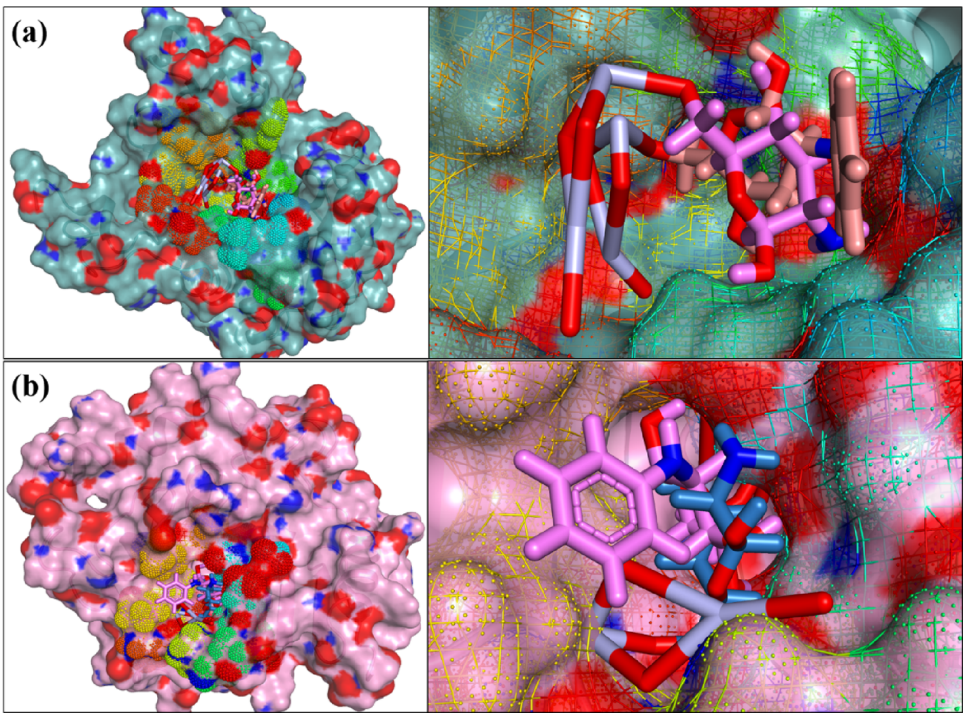

Figure 2. (a, b) 3D structural representation of synthesized CS-doped La_2O_3 and CS- and CDs-doped La_2O_3 inside the active pocket of $FabI_{E.\ coli}$ (a) and DNA $gyrase_{E.\ coli}$ (b).

using the diffusion method. Antibiotic discs were subjected to aseptic conditions on MacConkey agar swabbed with an activated growth of 1.5 × 108 CFU/mL (0.5 McFarland standard) and kept at 37 °C for 24 h. The 6 mm-diameter wells were drilled using a septic borer. Many concentrations of La_2O_3 and CDs/CS-doped La_2O_3 were applied as 1.0 mg/50 μL and 0.5 mg/50 μL. The +ve control was ciprofloxacin (0.005 mg/50 μL), and the −ve control was DI water (50 μL).[24] After overnight incubation at 37 °C, the bactericidal efficiency was calculated after analyzing inhibitory zones (mm) through the Vernier caliper.

2.5.5. Statistical Analysis. The antibacterial inhibitory zone (mm) size and diameters were statistically estimated using one-way ANOVA in SPSS 20.[25]

2.6. Molecular Docking Analysis. Molecular docking simulations were performed on enoyl-[acyl-carrier-protein] reductase (FabI) and DNA gyrase enzymes necessary for microbial survival.[26] The 3D structure for the chosen enzyme targets was retrieved from the protein database having PDB IDs 4D46 for $FabI_{E.\ coli}$[27] and 6KZV for $DNA\ gyrase_{E.\ coli}$.[28] Docking investigations were carried out using Sybyl X-2.0.[29,30] The protein structures were optimized by Sybyl's energy minimization tool after going through a multistep procedure that included, first, the removal of water molecules and native ligands and then added polar H-atoms with Gasteiger charges. The binding site was determined by defining a 5 Å around the native ligand. In each instance, the optimal docked posture of a stable complex was determined by generating the top 10 docked configurations. Ligand structures were created using the Sybyl sketch module tool by changing CS monomer structures obtained through PubChem, and stable conformations were constructed in this work. PyMOL 3D visualizers were utilized for analysis and graphical displays (Figure 2a,b).

3. RESULTS AND DISCUSSION

XRD was used to study the crystalline phase of pristine and incorporated La_2O_3 in the 2θ range of 10−70° indicated in Figure 3a. The XRD peaks at 2θ = 24.3° (100), 27.8° (002), 29.9° (011), 39.48° (012), 48.49° (111), and 55.39° (112) manifested to the hexagonal structure of La_2O_3 (JCPDS no. 04-0856[31] and JCPDS nos. 40-1279, 01-083-1344, and 73-2141),[32−34] respectively. The additional peaks were sited at 15.56° (020) and 20.26° ($\bar{1}$20) attributed to the monoclinic configuration of $La(NO_3)_3{\cdot}4H_2O$. There was no distinct dopant peak or alteration in the hexagonal structure of La_2O_3 upon CS doping. The widening of peaks resulted from CS incorporation, which was attributed to CS's synergistic impact and intermolecular interaction with NRs.[35] Upon CDs integration, more broadening of spacing was observed as the surface area of CDs varied from very small to large values;[36] thus, the intensity was affected by the nucleation during surface growth.

FTIR analysis of CDs/CS-doped NRs was used to evaluate the chemical composition and functional groups. The spectra ranged from 500 to 4000 cm^{-1}, depicted in Figure 3b. The peaks at 638, 845, and 1056 cm^{-1} exhibited the stretching vibration of the La−O bond.[37−39] A small peak at 3608 cm^{-1} and a strong peak at 1356 cm^{-1} can be due to the stretching and bending vibration of the OH bond in the water absorbed on the catalyst surface.[40,41] Upon doping, no additional peak was observed.

The electronic arrangement was estimated with electronic spectroscopy and E_g of formed NRs. The UV−vis spectra of the prepared La_2O_3 indicated an absorption band in the range of 270−300 nm (Figure 3c). The maximum wavelength at 275 nm was most likely caused by charge-transfer (O^{2-}/La^{3+}) absorption, which was attributed to the electronic transition $\pi-\pi^*$.[42] The E_g of La_2O_3 was found to be 4.3 eV, and only a slight decrease in the E_g was observed upon doping (e.g., ∼4.2

https://doi.org/10.1021/acsomega.3c02812
ACS Omega 2023, 8, 25401−25409

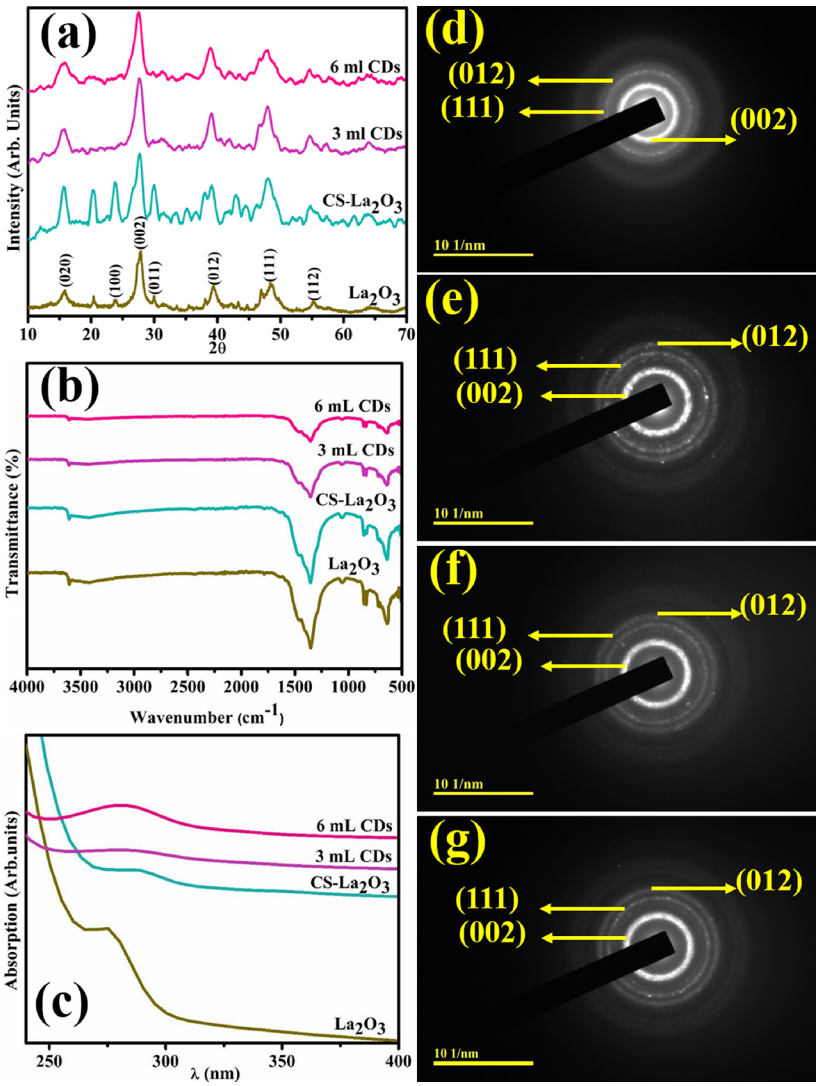

Figure 3. (a) XRD pattern, (b) FTIR spectra, (c) electronic spectra, and (d–g) SAED images of (d) La_2O_3, (e) CS-doped La_2O_3, (f) 3 mL of CDs/CS-doped La_2O_3, and (g) 6 mL of CDs/CS-doped La_2O_3.

eV). Absorption increased toward a higher wavelength upon CS and CDs doping; this slight shift in the center of the absorption band observed upon CS doping could be attributed to crystal structure defects caused by dopant ions.[43] The doped NCs decreased with crystallite size reduction due to poor orientation realignment and the crystalline nature of the resulting samples.[42] Based on the SAED pattern, it is evident that concentric rings associated with the planes (002), (111), and (012) of doped and undoped La2O3 corresponded to XRD data (Figure 3d–g).

EDS mapping was used to determine the chemical composition to validate the purity of the formed catalysts (Figure S1a–d). The pristine sample EDS spectrum confirmed that the formation of La and O as La_2O_3 and the C peak in the spectra was due to doping. The Na peaks resulted in NaOH being used as a precipitating agent during preparation to maintain the pH of the samples, while the spectral peaks of Au were found to reduce the charging effect of Au coating sprayed on NCs. In Figure S1e, the three specified elements (O, La, and C) have been evenly distributed throughout the sample, with varying elemental concentrations represented by various colors.

TEM was used to further characterize the microstructure with host morphology and CDs/CS-doped La_2O_3. The agglomerated rod-like structure of La_2O_3 can be seen in Figure 4a. Upon doping of CS, the NRs were encapsulated by CS, which seemed scattered on the surfaces of NRs with a high agglomeration (Figure 4b). In Figure 4c, the addition of CDs in the binary system (CS-La_2O_3) observed high-level aggregations of dopants with NRs. Functional groups on the surface of CDs, including hydroxyl, carboxyl, and amine, can interact and promote aggregation via hydrogen bonding.[44] A higher concentration of CDs revealed the reformation of small-sized NRs with comparatively less agglomeration (Figure 5d). The length and width of NRs changed from 56 to 43 nm and 6.2 to 3.9 nm upon doping, respectively.

HR-TEM was used to determine the periodic arrangement of atomic planes. The interlayer spacings of La_2O_3, CS-doped La_2O_3, and (3 and 6 mL) CDs/CS-doped La_2O_3 were calculated to be 0.18, 0.23, 0.32, and 0.32 nm corresponding to the XRD data elucidated in Figure S2a–d.

FESEM images of La_2O_3 and (3 and 6 mL) CDs/CS-doped La_2O_3 are demonstrated in Figure S3a–d. La_2O_3 revealed a nonuniform and aggregated NRs-like morphology (Figure

https://doi.org/10.1021/acsomega.3c02812
ACS Omega 2023, 8, 25401−25409

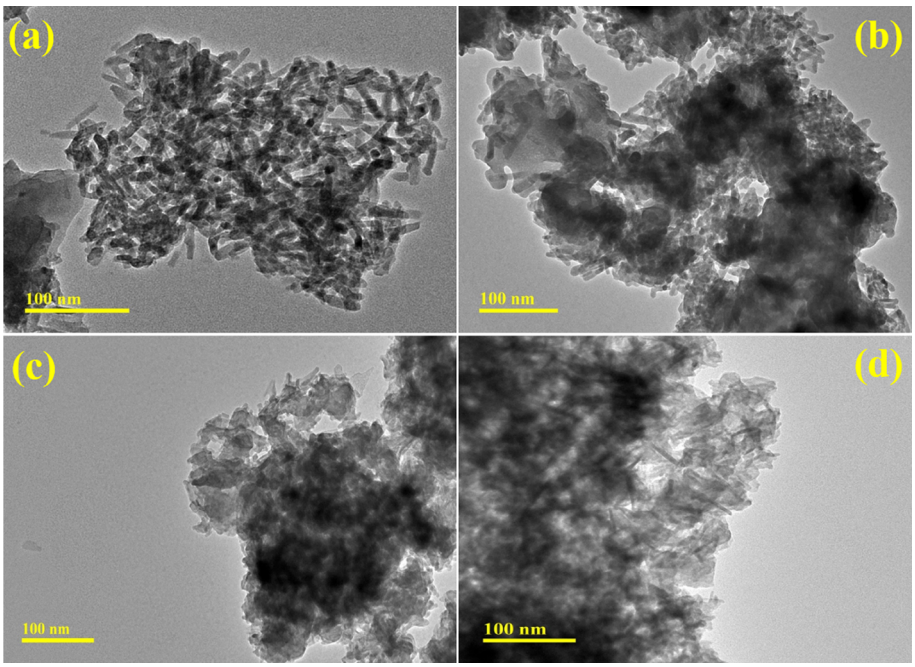

Figure 4. (a–d) TEM micrographs of (a) La_2O_3, (b) CS-doped La_2O_3, (c) 3 mL of CDs/CS-doped La_2O_3, and (d) 6 mL of CDs/CS-doped La_2O_3 NRs.

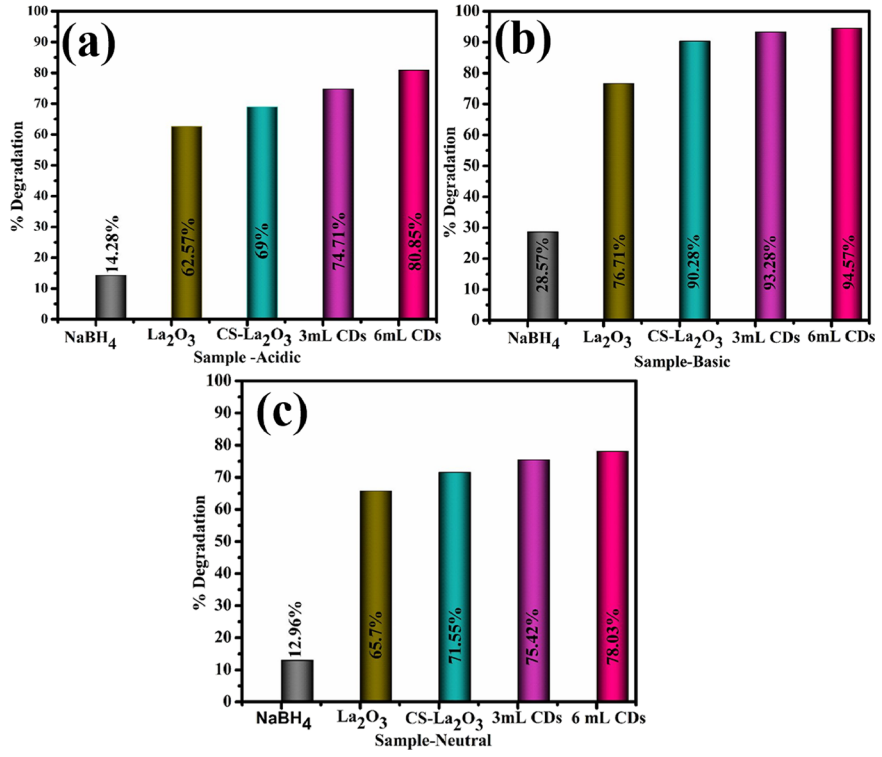

Figure 5. (a–c) CA of as-prepared NRs in (a) acidic, (b) basic, and (c) neutral media.

S3a). The incorporation of CS exhibited the formation chunk-like structure with the agglomeration of small-sized particles (Figure S3b). With CDs doping, partial overlapping of randomly oriented particles with chunks was observed (Figure S3c,d).

A UV–vis spectrophotometer was employed for RhB reduction of pure and incorporated specimens in the existence of $NaBH_4$. The RhB deterioration of all samples was 28.57–94.57% with pH ∼12; 14.28–80.85% in an environment with pH ∼2; and 12.96–78.03% in a medium with pH ∼7 in 10 min according to Figure 5a–c. $NaBH_4$ has advantages over more conventional methods in terms of speed, simplicity, convenience, and recyclability. The reaction is favorable thermodynamically but unfavorable kinetically without a catalyst. In an oxidation–reduction reaction, RhB accepts an e^- from the reducing agent while acting as an oxidizing agent.

https://doi.org/10.1021/acsomega.3c02812
ACS Omega 2023, 8, 25401–25409

The above reaction was time-consuming and exceptionally slow while being exposed to $NaBH_4$ in the absence of NCs. NCs (La_2O_3 and (3 and 6 mL) CDs/CS-doped La_2O_3) accelerate the transition of e^-s from the BH_4^- (donor) to the dye as H^+ (acceptor). Degradation becomes effective attributed to the higher number of active sites and RhB converted into LRhB. Following that, LRhB dye and BH_4^- were desorbed from the surface of the NCs (Figure 6). CA

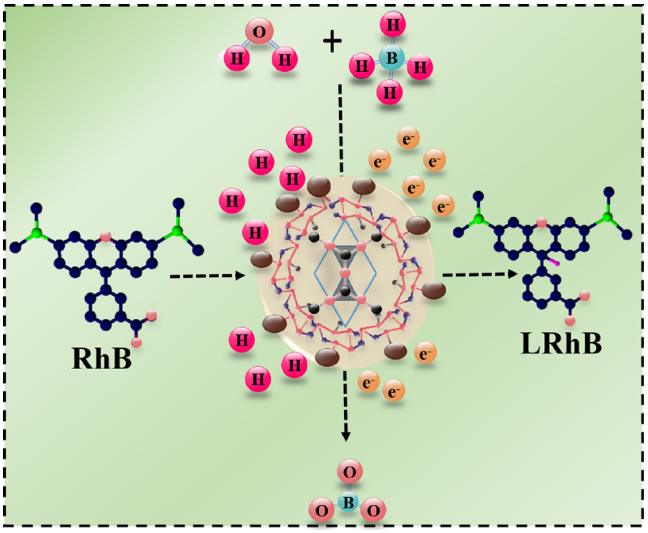

Figure 6. Mechanism of the CA of host and CDs/CS-doped La_2O_3 NRs.

functioned effectively in a basic environment ascribed to an enhanced electrostatic interaction between negatively charged NCs and positively charged dye. Thus, an enhancement in CA for all media was attributed to CDs, enhancing the surface-to-volume ratio for the reaction by the significant decrease in the particle size.[36] Dopant incorporation improved degradation ascribed to the inclusion of more active regions, resulting in a larger surface area for the catalyst.

Table 1 and Figure S4 show the antimicrobial efficacy of pure and integrated NRs against *E. coli* using a good diffusion

Table 1. Antibacterial Efficacy of CDs/CS-Doped La_2O_3

	inhibition zone (mm)	
sample	0.5 mg/50 μL	1.0 mg/50 μL
La_2O_3	1.90	2.80
CS-La_2O_3	2.15	2.55
3 mL of CDs	3.20	3.70
6 mL of CDs	3.55	4.15
ciprofloxacin	6.40	6.40
DI water	0	0

technique. The inhibition areas of *E. coli* for synthesized NRs were 0.35−2.95 and 1.75−3.45 mm for the higher (1.0 mg/50 L) and lower (0.5 mg/50 L) dosages, respectively, correspondingly. Compared to the DI water (negative control), the ciprofloxacin (positive control) demonstrated 5.35 mm inhibitory regions contrary to *E. coli*. The prominence of electrostatic interactions between negatively charged bacterial cell walls and this cationic molecule increases the antibactericidal potency upon CS doping.[45] Enhancement in the antibacterial action after incorporating CDs also contributed to CDs' extremely enormous surface area.[36]

The potential involvement of nanostructures as bactericidal agents has widely been documented; yet, the reason for their efficacy remains a mystery. The disruption of many cellular processes by antagonizing enzyme targets is regarded as a viable technique for discovering novel antibacterial drugs.[46,47] In the case of $FabI_{E.\ coli}$, both CS-doped La_2O_3 and CS- and CDs-doped La_2O_3 exhibited excellent binding scores of 4.76 and 5.50, respectively. Nine H-bonds, namely, Gly13, Ser19, Ile20, Ser91, Ile92, Gly93, Tyr156, Pro191, and Ile192, were the primary contributors to the formation of the docked complex in CS-doped La_2O_3 nanocomposites (Figure 7a,b).

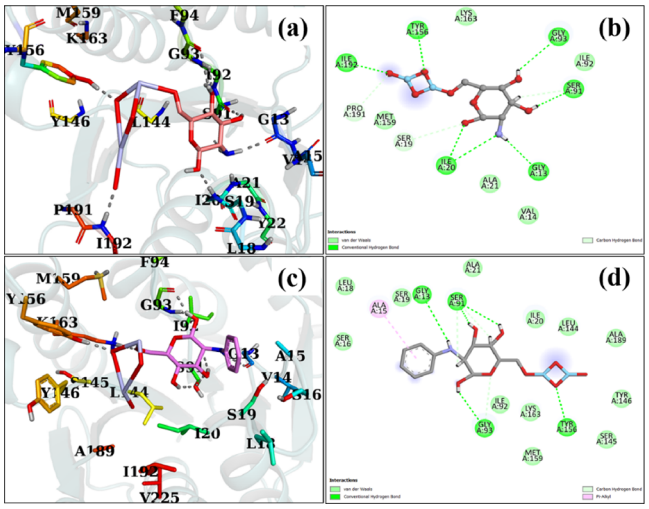

Figure 7. (a−d) Binding interaction pattern inside the active pocket of FabI from *E. coli* (a, b) CS-doped La_2O_3 and (c, d) CS- and CDs-doped La_2O_3.

Similarly, the CS- and CDs-doped La_2O_3 complex with $FabI_{E.\ coli}$ exhibited numerous H-bonds involving Gly13, Ser91, Gly93, Tyr156, and Lys163 in addition to hydrophobic contacts involving Ala15, as illustrated in Figure 7c,d.

Another enzyme target chosen was DNA gyrase, required for bacterial survival, which has been identified as a significant target for discovering novel antibiotics. Both CS-doped La_2O_3 and CS- and CDs-doped La_2O_3 were examined for binding mechanism and propensity for complex formation inside the active region for *E. coli* DNA gyrase. CS-doped La_2O_3 had a binding score of 5.39 for H-bond interactions with Asn46, Asp73, Gly77, and Thr165 (Figure 8a,b). Similarly, the CS- and CDs-doped La_2O_3 docked complex Asn46, Val71, Asp73, and Val167 exhibited four H-bonds and pi−pi interactions with Ile78, Pro79, and Ile94 (Figure 8c,d).

4. CONCLUSIONS

A coprecipitation route efficiently synthesized diverse CDs concentrations in constant quantities of CS-doped La_2O_3 nanostructures to test antibacterial action and catalytic potency. The XRD spectra indicated that La_2O_3 had a hexagonal and cubic structure with no variations. Identifying functional groups at 1056 and 638 cm^{-1} confirmed the La_2O_3 using FTIR, while bright dots determined crystallinity in SAED. The UV−vis spectrophotometer depicts a significant decrease in E_g energy and redshift in the electronic spectra upon doping. In the sample, the presence of a dopant was

https://doi.org/10.1021/acsomega.3c02812
ACS Omega 2023, 8, 25401−25409

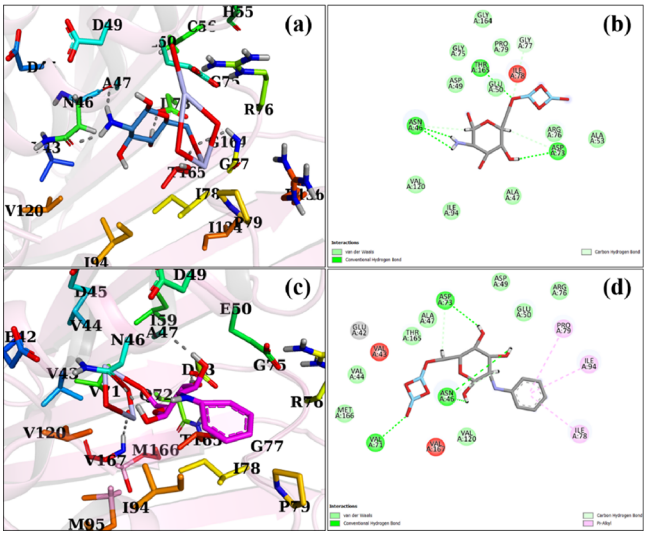

Figure 8. (a–d) Binding interaction pattern inside the active pocket of DNA gyrase from *E. coli* (a, b) CS-doped La_2O_3 and (c, d) CS- and CDs-doped La_2O_3.

confirmed using EDS spectroscopy. HR-TEM determined the d-spacing (0.18, 0.23, 0.32, and 0.32 nm) corresponding with XRD. In the basic medium for CDs/CS-doped La_2O_3, the maximal catalytic degradation of RhB was recorded at 94.57%. Furthermore, the bactericidal efficiency of the NRs for the *E. coli* (0–4.15 mm) and their mechanism for enoyl-[acyl-carrier-protein] reductase (FabI) and DNA gyrase enzyme was assessed by in silico studies. Based on these findings, we infer that CDs-doped La_2O_3 may be employed as a potential inhibitor.

■ ASSOCIATED CONTENT

Data Availability Statement

The data will be available from the corresponding author on request.

Supporting Information

The Supporting Information is available free of charge at https://pubs.acs.org/doi/10.1021/acsomega.3c02812.

EDS spectra, interlayer d-spacing, SEM images, and mechanism of antibacterial activity (Figures S1–S4) (PDF)

■ AUTHOR INFORMATION

Corresponding Authors

Muhammad Imran − *Department of Chemistry, Government College University, Sahiwal, Punjab 57000, Pakistan*; Email: imran@mail.ipc.ac.cn

Ali Haider − *Department of Clinical Sciences, Faculty of Veterinary and Animal Sciences,, Muhammad Nawaz Shareef University of Agriculture, Multan 66000 Punjab, Pakistan*; Email: ali.haider@mnsuam.edu.pk

Ali Al-Shanini − *College of Petroleum and Engineering, Hadhramout University, Mukalla, Hadhramout 50511, Yemen*; orcid.org/0000-0002-7616-7814; Email: a.alshanini@hu.edu.ye

Muhammad Ikram − *Solar Cell Applications Research Lab, Department of Physics, Government College University Lahore, Lahore 54000 Punjab, Pakistan*; orcid.org/0000-0001-7741-789X; Email: dr.muhammadikram@gcu.edu.pk

Authors

Sumaira Rasool − *Department of Chemistry, Government College University, Sahiwal, Punjab 57000, Pakistan*

Anum Shahzadi − *Faculty of Pharmacy, The University of Lahore, Lahore 54000, Pakistan*

Walid Nabgan − *Departament d'Enginyeria Química, Universitat Rovira i Virgili, 43007 Tarragona, Spain*; orcid.org/0000-0001-9901-862X

Iram Shahzadi − *Punjab University College of Pharmacy, University of the Punjab, Lahore 54000, Pakistan*

Francisco Medina − *Departament d'Enginyeria Química, Universitat Rovira i Virgili, 43007 Tarragona, Spain*; orcid.org/0000-0002-3111-1542

Mohammed M. Algaradah − *Chemistry Department, King Khalid Military Academy, Riyadh 11495, Saudi Arabia*

Ahmed M. Fouda − *Chemistry Department, Faculty of Science, King Khalid University, Abha 61413, Saudi Arabia*

Complete contact information is available at: https://pubs.acs.org/10.1021/acsomega.3c02812

Notes

The authors declare no competing financial interest.

■ ACKNOWLEDGMENTS

The authors are grateful to HEC, Pakistan, through NRPU 20-17615 and extend their appreciation to the Deanship of Scientific Research at King Khalid University, Saudi Arabia, for funding this work through Small Groups Project under grant number (RGP.1/248/44).

■ REFERENCES

(1) Busch, M. A. Chiral Pollutants: Distribution, Toxicity and Analysis by Chromatography and Capillary Electrophoresis By Imran Ali (National Institute of Hydrology, Roorkee, India) and Hassan Y. Aboul-Enein (King Faisal Specialist Hospital, Riyadh, Saudi Arabia). John W. *J. Am. Chem. Soc.* **2004**, *126*, 14680.

(2) Jiao, M.; Yao, Y.; Chen, C.; Jiang, B.; Pastel, G.; Lin, Z.; Wu, Q.; Cui, M.; He, S.; Hu, L. Highly Efficient Water Treatment via a Wood-Based and Reusable Filter. *ACS Mater. Lett.* **2020**, *2*, 430–437.

(3) Lonnen, J.; Kilvington, S.; Kehoe, S. C.; Al-Touati, F.; McGuigan, K. G. Solar and Photocatalytic Disinfection of Protozoan, Fungal and Bacterial Microbes in Drinking Water. *Water Res.* **2005**, *39*, 877–883.

(4) Ikram, M.; Shahzadi, I.; Haider, A.; Hayat, S.; Haider, J.; Ul-Hamid, A.; Shahzadi, A.; Nabgan, W.; Dilpazir, S.; Ali, S. Improved Catalytic Activity and Bactericidal Behavior of Novel Chitosan/V_2O_5 Co-Doped in Tin-Oxide Quantum Dots. *RSC Adv.* **2022**, *12*, 23129–23142.

(5) Rambabu, K.; Bharath, G.; Banat, F.; Show, P. L. Green Synthesis of Zinc Oxide Nanoparticles Using Phoenix Dactylifera Waste as Bioreductant for Effective Dye Degradation and Antibacterial Performance in Wastewater Treatment. *J. Hazard. Mater.* **2021**, *402*, No. 123560.

(6) Xian, Y.; Gao, F.; Cai, B. Synthesis of Platinum Nanoparticle Chains Based on α-Chymotrpsin Fibrils. *Mater. Lett.* **2013**, *111*, 39–42.

(7) Farrukh, M. A.; Imran, F.; Ali, S.; Khaleeq-Ur-Rahman, M.; Naqvi, I. I. Micelle Assisted Synthesis of La2O3 Nanoparticles and Their Applications in Photodegradation of Bromophenol Blue. *Russ. J. Appl. Chem.* **2015**, *88*, 1523–1527.

(8) Xie, Y.; Wu, J.; Sun, C.; Ling, Y.; Li, S.; Li, X.; Zhao, J.; Yang, K. La_2O_3-Modified Graphite Carbon Nitride Achieving the Enhanced

Photocatalytic Degradation of Different Organic Pollutants under Visible Light Irradiation. *Mater. Chem. Phys.* **2020**, *246*, No. 122846.
(9) Almarri, M. N.; Khalaf, M. M.; Gouda, M.; El-Taib Heakal, F.; Elmushyakhi, A.; Abou Taleb, M. F.; Abd El-Lateef, H. M. Chemical, Surface, and Thermal Studies of Mixed Oxides Cupric Oxide (CuO), Lanthanum Oxide (La_2O_3), and Graphene Oxide for Superior Dye Degradation from Aqueous Solution. *J. Mater. Res. Technol.* **2023**, 2263.
(10) Jbeli, R.; Lahmar, M.; Bilel, C.; Saadallah, F.; Ouzari, H. I.; Bouaïcha, M.; Amlouk, M. Structural and Optical Investigations on Sprayed Co Doped La_2O_3 Thin Films along with Photocatalytic and Anti-Bacterial Applications. *Optik (Stuttgart, Ger.)* **2021**, *242*, No. 166837.
(11) Maria Magdalane, C.; Kaviyarasu, K.; Matinise, N.; Mayedwa, N.; Mongwaketsi, N.; Letsholathebe, D.; Mola, G. T.; AbdullahAl-Dhabi, N.; Arasu, M. V.; Henini, M.; Kennedy, J.; Maaza, M.; Jeyaraj, B. Evaluation on La_2O_3 Garlanded Ceria Heterostructured Binary Metal Oxide Nanoplates for UV/Visible Light Induced Removal of Organic Dye from Urban Wastewater. *S. Afr. J. Chem. Eng.* **2018**, *26*, 49−60.
(12) Arshad, A.; Siddique, S.; Shahid, M.; Zulqurnain, M.; Niazi, R. K.; Mansoor, Q.; Nadeem, K. Bi-Functional Ni-Doped La2O3nanosheets: Their Enhanced Photocatalytic Performance and Antibacterial Properties. *J. Phys. D: Appl. Phys.* **2022**, *55*, 304007.
(13) He, Y. W.; Yin, Y. B.; Chang, T.; Bian, L.; Zhang, G. Q.; Li, X. L. A Facile Synthesis of La_2O_3/GO Nanocomposites in N,N-Dimethylformamide with High Dye Degradation Efficiency. *J. Nanomater.* **2018**, *2018*, 1.
(14) Moeen, S.; Ikram, M.; Haider, A.; Haider, J.; Ul-Hamid, A.; Nabgan, W.; Shujah, T.; Naz, M.; Shahzadi, I. Comparative Study of Sonophotocatalytic, Photocatalytic, and Catalytic Activities of Magnesium and Chitosan-Doped Tin Oxide Quantum Dots. *ACS Omega* **2022**, *7*, 46428−46439.
(15) Shahabuddin, S.; Sarih, N. M.; Ismail, F. H.; Shahid, M. M.; Huang, N. M. Synthesis of Chitosan Grafted-Polyaniline/Co_3O_4 Nanocube Nanocomposites and Their Photocatalytic Activity toward Methylene Blue Dye Degradation. *RSC Adv.* **2015**, *5*, 83857−83867.
(16) Rani, M.; Rachna; Shanker, U. Metal Oxide-Chitosan Based Nanocomposites for Efficient Degradation of Carcinogenic PAHs. *J. Environ. Chem. Eng.* **2020**, *8*, No. 103810.
(17) Zhang, J.; Ding, E.; Xu, S.; Li, Z.; Fakhri, A.; Gupta, V. K. Production of Metal Oxides Nanoparticles Based on Poly-Alanine/Chitosan/Reduced Graphene Oxide for Photocatalysis Degradation, Anti-Pathogenic Bacterial and Antioxidant Studies. *Int. J. Biol. Macromol.* **2020**, *164*, 1584−1591.
(18) Wang, J.; Zhang, H.; Zhang, K.; Pal, N. R. Bilateral Sensitivity Analysis for Understandable Neural Networks and Its Application to Reservoir Engineering. 2020, 1−12.
(19) Thi Hoan, B.; Dinh Tam, P.; Pham, V.-H. Green Synthesis of Highly Luminescent Carbon Quantum Dots from Lemon Juice. *J. Nanotechnol.* **2019**, 2852816.
(20) Sinclair, C. G. Bergey's Manual of Determinative Bacteriology. *Am. J. Trop. Med. Hyg.* **1939**, *s1-19*, 605−606.
(21) Adzitey, F.; Yussif, S.; Ayamga, R.; Zuberu, S.; Addy, F.; Adu-Bonsu, G.; Huda, N.; Kobun, R. Antimicrobial Susceptibility and Molecular Characterization of Escherichia Coli Recovered from Milk and Related Samples. *Microorganisms* **2022**, *10*, 1335.
(22) NCCLS. Performance Standards for Antimicrobial Susceptibility Testing. *Clin. Lab. Standars Inst.* **2022**, *27*, 1−182.
(23) Iwalokun, B. A.; Ogunledun, A.; Ogbolu, D. O.; Bamiro, S. B.; Jimi-Omojola, J. In Vitro Antimicrobial Properties of Aqueous Garlic Extract against Multidrug-Resistant Bacteria and Candida Species from Nigeria. *J. Med. Food* **2004**, *7*, 327−333.
(24) Haider, A.; Ijaz, M.; Imran, M.; Naz, M.; Majeed, H.; Khan, J. A.; Ali, M. M.; Ikram, M. Enhanced Bactericidal Action and Dye Degradation of Spicy Roots' Extract-Incorporated Fine-Tuned Metal Oxide Nanoparticles. *Appl. Nanosci.* **2020**, *10*, 1095−1104.
(25) Haider, A.; Ijaz, M.; Ali, S.; Haider, J.; Imran, M.; Majeed, H.; Shahzadi, I.; Ali, M. M.; Khan, J. A.; Ikram, M. Green Synthesized Phytochemically (*Zingiber Officinale* and *Allium Sativum*) Reduced Nickel Oxide Nanoparticles Confirmed Bactericidal and Catalytic Potential. *Nanoscale Res. Lett.* **2020**, *15*, 50.
(26) Ikram, M.; Haider, A.; Imran, M.; Haider, J.; Naz, S.; Ul-Hamid, A.; Nabgan, W.; Mustajab, M.; Shahzadi, A.; Shahzadi, I.; Raza, M. A.; Nazir, G. Facile Synthesis of Starch and Tellurium Doped SrO Nanocomposite for Catalytic and Antibacterial Potential: In Silico Molecular Docking Studies. *Int. J. Biol. Macromol.* **2022**, *221*, 496−507.
(27) Schiebel, J.; Chang, A.; Merget, B.; Bommineni, G. R.; Yu, W.; Spagnuolo, L. A.; Baxter, M. V.; Tareilus, M.; Tonge, P. J.; Kisker, C.; Sotriffer, C. A. An Ordered Water Channel in Staphylococcus Aureus FabI: Unraveling the Mechanism of Substrate Recognition and Reduction. *Biochemistry* **2015**, *54*, 1943−1955.
(28) Ushiyama, F.; Amada, H.; Takeuchi, T.; Tanaka-Yamamoto, N.; Kanazawa, H.; Nakano, K.; Mima, M.; Masuko, A.; Takata, I.; Hitaka, K.; Iwamoto, K.; Sugiyama, H.; Ohtake, N. Lead Identification of 8-(Methylamino)-2-Oxo-1,2-Dihydroquinoline Derivatives as DNA Gyrase Inhibitors: Hit-to-Lead Generation Involving Thermodynamic Evaluation. *ACS Omega* **2020**, *5*, 10145−10159.
(29) Shahzadi, I.; Islam, M.; Saeed, H.; Haider, A.; Shahzadi, A.; Haider, J.; Ahmed, N.; Ul-Hamid, A.; Nabgan, W.; Ikram, M.; Rathore, H. A. Formation of Biocompatible MgO/Cellulose Grafted Hydrogel for Efficient Bactericidal and Controlled Release of Doxorubicin. *Int. J. Biol. Macromol.* **2022**, *220*, 1277−1286.
(30) Mehmood, Z.; Ikram, M.; Imran, M.; Shahzadi, A.; Haider, A.; Ul-Hamid, A.; Nabgan, W.; Haider, J.; Hayat, S. Z. officinale-doped silver/calcium oxide nanocomposites: Catalytic activity and antimicrobial potential with molecular docking analysis. *Process Biochem.* **2022**, *121*, 635−646.
(31) Pathan, A. A.; Desai, K. R.; Vajapara, S.; Bhasin, C. P. Conditional Optimization of Solution Combustion Synthesis for Pioneered La_2O_3 Nanostructures to Application as Future CMOS and NVMS Generations. *Adv. Nanopart.* **2018**, *07*, 28−35.
(32) Qu, S.; Yu, Y.; Lin, K.; Liu, P.; Zheng, C.; Wang, L.; Xu, T.; Wang, Z.; Wu, H. Easy Hydrothermal Synthesis of Multi-Shelled La_2O_3 Hollow Spheres for Lithium-Ion Batteries. *J. Mater. Sci.: Mater. Electron.* **2018**, *29*, 1232−1237.
(33) Ghelamallah, M.; Granger, P. Supported-induced effect on the catalytic properties of Rh and Pt-Rh particles deposited on La_2O_3 and mixed α-Al_2O_3-La_2O_3 in the dry reforming of methane. *Appl. Catal., A* **2014**, *485*, 172−180.
(34) Long, Y.; Yang, J.; Li, X.; Huang, W.; Tang, Y.; Zhang, Y. Combustion Synthesis and Stability of Nanocrystalline La2O 3 via Ethanolamine-Nitrate Process. *J. Rare Earths* **2012**, *30*, 48−52.
(35) Weng, Y.; Deng, D.; Zhang, L.; Su, Y.; Lv, Y. A Cataluminescence Gas Sensor Based on Mesoporous Mg-Doped SnO_2 Structures for Detection of Gaseous Acetone. *Anal. Methods* **2016**, *8*, 7816−7823.
(36) Deshmukh, A. A.; Mhlanga, S. D.; Coville, N. J. Carbon Spheres. *Materials Science and Engineering R: Reports*; Elsevier Ltd September 2010, pp. 1−28. DOI: 10.1016/j.mser.2010.06.017.
(37) Karthikeyan, S.; Selvapandiyan, M.; Shanavas, S.; Anbarasan, P. M.; Acevedo, R. A Role of Annealing Temperature on the Properties of Lanthanum Oxide (La_2O_3) Microplates by Reflux Routes. *Mater. Today: Proc.* **2020**, *26*, 3576−3578.
(38) Gangwar, B. P.; Palakollu, V.; Singh, A.; Kanvah, S.; Sharma, S. Combustion Synthesized La_2O_3 and $La(OH)_3$: Recyclable Catalytic Activity towards Knoevenagel and Hantzsch Reactions. *RSC Adv.* **2014**, *4*, 55407−55416.
(39) Ravi, G.; Sarasija, M.; Ayodhya, D.; Kumari, L. S.; Ashok, D. Facile Synthesis, Characterization and Enhanced Catalytic Reduction of 4-Nitrophenol Using $NaBH_4$ by Undoped and Sm^{3+}, Gd^{3+}, Hf^{3+} Doped La_2O_3 Nanoparticles. *Nano Converg.* **2019**, *6*, 12.
(40) Le Van, T.; Che, M.; Tatibouët, J. M.; Kermarec, M. Infrared Study of the Formation and Stability of $La_2O_2CO_3$ during the Oxidative Coupling of Methane on La_2O_3. *J. Catal.* **2019**, *142*, 18−26.

https://doi.org/10.1021/acsomega.3c02812
ACS Omega 2023, 8, 25401−25409

(41) Mu, Q.; Wang, Y. Synthesis, Characterization, Shape-Preserved Transformation, and Optical Properties of La(OH)3, La2O2CO3, and La2O3 Nanorods. *J. Alloys Compd.* **2011**, *509*, 396−401.
(42) Ikram, M.; Abid, N.; Haider, A.; Ul-Hamid, A.; Haider, J.; Shahzadi, A.; Nabgan, W.; Goumri-Said, S.; Butt, A. R.; Benali Kanoun, M. Toward Efficient Dye Degradation and the Bactericidal Behavior of Mo-Doped La2O3nanostructures. *Nanoscale Adv.* **2022**, *4*, 926−942.
(43) Ikram, M.; Shujait, S.; Haider, A.; Kashaf-Ul-Ain; Ul-Hamid, A.; Haider, J.; Shahzadi, I.; Nabgan, W.; Imran, M.; Butt, A. R. Molybdenum and Chitosan-Doped MnO_2 Nanostructures Used as Dye Degrader and Antibacterial Agent. *Appl. Nanosci.* **2022**, *12*, 3909−3924.
(44) Ankireddy, S. R.; Vo, V. G.; An, S. S. A.; Kim, J. Solvent-Free Synthesis of Fluorescent Carbon Dots: An Ecofriendly Approach for the Bioimaging and Screening of Anticancer Activity via Caspase-Induced Apoptosis. *ACS Appl. Bio Mater.* **2020**, *3*, 4873−4882.
(45) Ke, C. L.; Deng, F. S.; Chuang, C. Y.; Lin, C. H. Antimicrobial Actions and Applications of Chitosan. *Polymer* **2021**, DOI: 10.3390/polym13060904.
(46) Ikram, M.; Chaudhary, K.; Shahzadi, A.; Haider, A.; Shahzadi, I.; Ul-Hamid, A.; Abid, N.; Haider, J.; Nabgan, W.; Butt, A. R. Chitosan/Starch-Doped MnO_2 Nanocomposite Served as Dye Degradation, Bacterial Activity, and Insilico Molecular Docking Study. *Mater. Today Nano* **2022**, *20*, No. 100271.
(47) Shujah, T.; Shahzadi, A.; Haider, A.; Mustajab, M.; Haider, A. M.; Ul-Hamid, A.; Haider, J.; Nabgan, W.; Ikram, M. Molybdenum-Doped Iron Oxide Nanostructures Synthesized via a Chemical Co-Precipitation Route for Efficient Dye Degradation and Antimicrobial Performance: In Silico Molecular Docking Studies. *RSC Adv.* **2022**, *12*, 35177−35191.

https://doi.org/10.1021/acsomega.3c02812
ACS Omega 2023, 8, 25401−25409